Compressibility of copper-oxygen bonds: a high-pressure neutron powder diffraction study of CuO

1999 J. Phys.: Condens. Matter 11 6501

(http://iopscience.iop.org/0953-8984/11/34/301)

J. Phys.: Condens. Matter **11** (1999) 6501–6508. Printed in the UK PII: S0953-8984(99)02836-2

Compressibility of copper–oxygen bonds: a high-pressure neutron powder diffraction study of CuO

H Ehrenberg†, J A McAllister†‡, W G Marshall§ and J P Attfield†‡

† Interdisciplinary Research Centre in Superconductivity, Madingley Road, Cambridge CB3 0HE, UK

‡ Department of Chemistry, University of Cambridge, Lensfield Road, Cambridge CB2 1EW, UK

§ ISIS Neutron Facility, CLRC Rutherford Appleton Laboratory, Chilton, Didcot, Oxon OX11 0QX, UK

Received 22 March 1999, in final form 4 June 1999

Abstract. A high-pressure neutron powder diffraction study has been performed on CuO at room temperature for nine different pressures up to 8.8 GPa. Rietveld refinement gives very precise atomic parameters, enabling the copper–oxygen bond compressibility to be determined accurately. The Jahn–Teller elongated bond distance obeys $\kappa_{Cu-O}(p) = 0.0710(55)/(p + 3.15(55)$ GPa) and is compared with the Cu–O bond compressibility in other materials. A Birch equation of state fitted to the experimental cell volume data gives $K_0 = 72(2)$ GPa, $K_0' = 8.7(1.2)$ and $V_0 = 80.89(5)$ Å^3.

1. Introduction

The compressibility of copper–oxygen bonds plays a crucial role in the structure–property relationships of high-T_C superconductors, e.g. with respect to pressure-induced charge transfer in $YBa_2Cu_3O_{7-x}$ [1], the effect of bond-length mismatch in $Ln_{2-x}Ce_xCuO_4$ (Ln = lanthanide) [2] and the ionic–covalent character of Cu–O bonds [3]. The application of external pressure also has a strong influence on the structural behaviour of the spin–Peierls system $CuGeO_3$ as summarized in the p–T phase diagram [4]. However, for a systematic study of Cu(II)–O bond compressibility, all compounds of major physical interest have the disadvantage of being at least ternary systems with different types of elements forming bonds. Hence, CuO itself is the most suitable system for this purpose. CuO crystallizes in the monoclinic space group $C2/c$, with Cu on the (4c) site $(\frac{1}{4}, \frac{1}{4}, 0)$ and oxygen on the (4e) site $(0, y, \frac{1}{4})$ [5, 6]. The $[CuO_6]$ octahedron is highly distorted due to the Jahn–Teller effect—see figure 1—and the inequivalent O–Cu–O bond angles α_1, α_2 and α_3 deviate strongly from 90°. The calculation of the copper–oxygen bond lengths requires the accurate determination of the atomic parameter y(O) as well as the four variable cell parameters.

Previous work on CuO at high pressure has been performed on a single crystal using synchrotron radiation [7], but no values for the atomic parameter of the oxygen, y(O), were determined. The pressure dependence of the three Raman-active optical modes has indicated that y(O) decreases with pressure, and a pressure dependence of $\partial y(O)/\partial p = -0.0025(5)$ GPa^{-1} was proposed to give agreement between the observed energy shifts and a simple force-constant model up to 8 GPa [8]. However, the observed decrease in y(O) obtained at a single pressure (2.2(1) GPa) in the only previous high-pressure neutron powder experiment [9] suggested a value for $\partial y(O)/\partial p$ which was more than three times larger than

0953-8984/99/346501+08$30.00

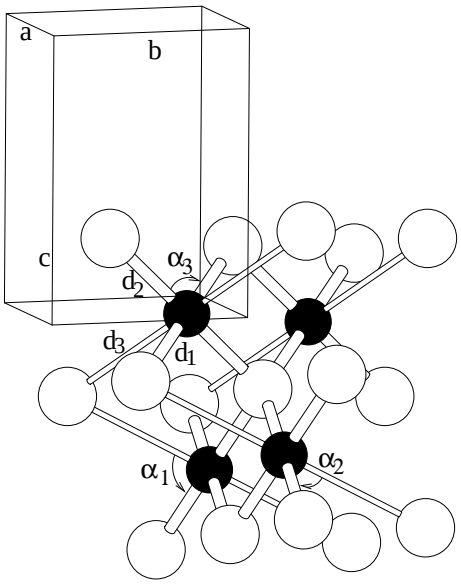

Figure 1. A section of the crystal structure of CuO. The filled circles are Cu ions, surrounded by highly distorted oxygen octahedra.

the above. In this paper we report the results of a new neutron powder diffraction study at room temperature for nine different pressures from 0.15 to 8.8 GPa, so providing suitable experimental data for a systematic study of the compressibility of copper–oxygen bonds. The values obtained are compared with those for some other copper oxides.

2. Experimental procedure

The present high-pressure time-of-flight (TOF) neutron powder diffraction study was conducted at the PEARL/HiPr high-pressure station of the ISIS Neutron Facility at CLRC Rutherford Appleton Laboratory, UK. The sample, CuO (Aldrich, 99.99+%), was thoroughly mixed with the NaCl (Aldrich, 99.999%) pressure standard in the volume ratio 2:1. This ratio was chosen as a compromise between ensuring good stress continuity between the crystallites of the two component phases and the requirement to have at least comparable peak intensities in the resulting neutron diffraction pattern. This mixture was pressed to a pellet of 6.0 mm diameter and about 1.6 mm height, which was then loaded into a V4-type Paris–Edinburgh pressure cell equipped with standard tungsten carbide anvils [10]. Prior to sealing the cell the sample was thoroughly moistened using the Fluorinert pressure-transmitting medium. Room temperature time-of-flight neutron diffraction data were then collected at nine pressures up to 8.8 GPa using the three main transverse scattering geometry detector banks centred at $2\theta = 90^\circ$. The final diffraction patterns were obtained by focusing the individual detector element spectra, normalizing the focused patterns with respect to the incident beam monitor and the scattering from a standard vanadium sample, and correcting for the wavelength and scattering-angle dependence of the neutron attenuation by the anvil (WC) and gasket (TiZr) materials [11]. Full-profile Rietveld refinements of the resulting patterns were then carried out using the GSAS package [12]. Sample pressures were determined from the NaCl equation

of state [13] using the refined lattice parameters and the measured ambient pressure value $a_0 = 5.63186(20)$ Å.

3. Results and discussion

A summary of the refined CuO structural parameters and the derived copper–oxygen bond lengths are shown in tables 1 and 2, respectively. Figure 2 illustrates a representative sample of the data, showing the observed and calculated profiles and the difference curve for the lowest and highest pressures under consideration. The pressure dependence of the cell parameters and other structural quantities f can be fitted by a power series in pressure p up to second order

$$f(p) = f_0 + f_1 p + f_2 p^2 \tag{1}$$

and the coefficients are summarized in table 3.

Table 1. Structural parameters of CuO at room temperature as obtained from the TOF neutron powder diffraction data by Rietveld refinement.

p (GPa)	a (Å)	b (Å)	c (Å)	β (deg)	V (Å^3)	y(O)
0.148(4)	4.6798(5)	3.4124(3)	5.1231(5)	99.525(6)	80.699(8)	0.4161(7)
1.505(5)	4.6950(5)	3.3668(4)	5.1036(5)	100.286(7)	79.377(9)	0.4035(6)
2.297(6)	4.7049(6)	3.3390(5)	5.0933(6)	100.703(10)	78.623(12)	0.3997(7)
3.243(16)	4.7140(9)	3.3093(7)	5.0838(9)	101.117(10)	77.818(31)	0.3949(6)
4.257(24)	4.7183(11)	3.2855(9)	5.0744(11)	101.487(14)	77.088(39)	0.3898(7)
5.208(48)	4.7232(10)	3.2624(8)	5.0646(10)	101.807(12)	76.388(32)	0.3864(7)
6.378(13)	4.7252(7)	3.2390(6)	5.0552(8)	102.000(12)	75.677(13)	0.3829(6)
7.491(33)	4.7300(12)	3.2201(10)	5.0483(12)	102.248(15)	75.139(41)	0.3814(8)
8.765(17)	4.7297(9)	3.1986(7)	5.0382(9)	102.494(14)	74.416(15)	0.3772(8)

Table 2. Copper–oxygen bond lengths in CuO, based on the structural parameters in table 1.

p (GPa)	d_1 (Å)	d_2 (Å)	d_3 (Å)
0.148(4)	1.9559(7)	1.9522(13)	2.7711(19)
1.505(5)	1.9513(6)	1.9575(12)	2.7041(17)
2.297(6)	1.9522(6)	1.9536(13)	2.6748(18)
3.243(16)	1.9524(6)	1.9512(12)	2.6423(17)
4.257(24)	1.9514(7)	1.9506(12)	2.6122(20)
5.208(48)	1.9512(6)	1.9474(14)	2.5878(18)
6.378(13)	1.9490(5)	1.9457(12)	2.5639(16)
7.491(33)	1.9502(7)	1.9408(16)	2.5478(21)
8.765(17)	1.9480(6)	1.9396(15)	2.5230(20)

The pressure-induced changes of the lattice parameters agree only qualitatively with those reported for a single-crystal synchrotron study [7]—see figure 3—as the proposed linear increase of a up to 8 GPa is not confirmed and the curvature of $c(p)$ is different as c_2 has a different sign. Details of the method and reliability of lattice parameter determination are not provided in [7], so our values, obtained from Rietveld analysis of neutron data, may be more reliable.

The y(O) variation is significantly non-linear, in contrast to the linear decrease up to 8 GPa proposed in [8]; see figure 4. Also, an extrapolation of the low-pressure value of

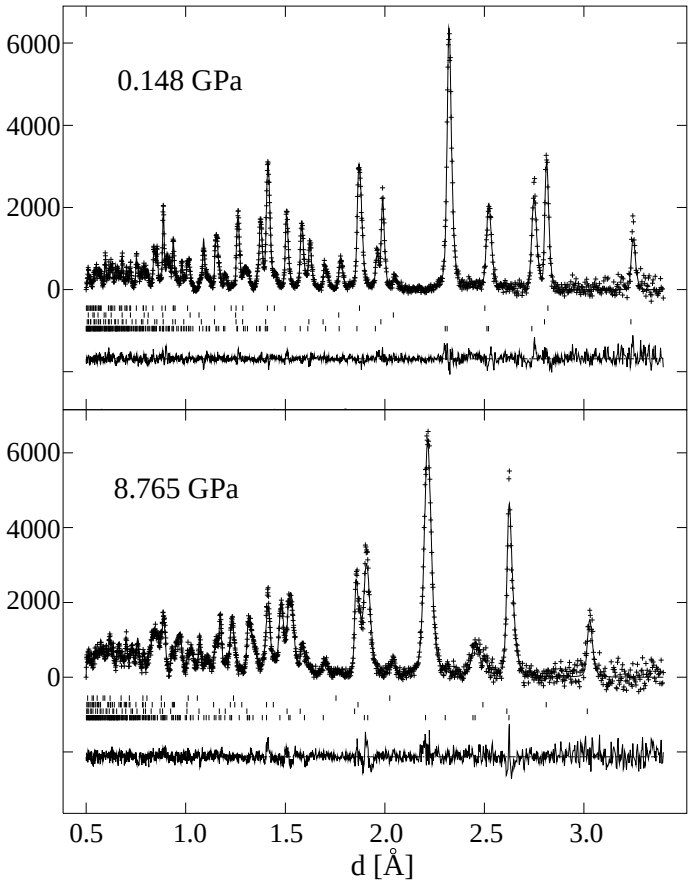

Figure 2. Observed and calculated profiles at the lowest and highest pressure under consideration. The lines of reflection marks belong to CuO, NaCl, Ni and WC from bottom to top. The latter two are very small contributions from the pressure cell anvil material (tungsten carbide with Ni binder).

Table 3. Coefficients for the pressure dependence of structural parameters f according to equation (1).

Parameter f	f_0	f_1 (10^{-3} GPa^{-1})	f_2 (10^{-6} GPa^{-2})
a (Å)	4.6786	12.83	−808.5
b (Å)	3.4176	−37.04	1395
c (Å)	5.1242	−13.98	490.5
β (deg)	99.462	59.7	−2930
y(O)	0.4160	−7.83	405
d_1 (Å)	1.9543	−0.691	0
d_2 (Å)	1.9571	−1.91	0
d_3 (Å)	2.7739	−47.21	2180
α_1 (deg)	88.866	59.93	0
α_2 (deg)	73.546	872.0	−39800
α_3 (deg)	95.565	−177.0	6700

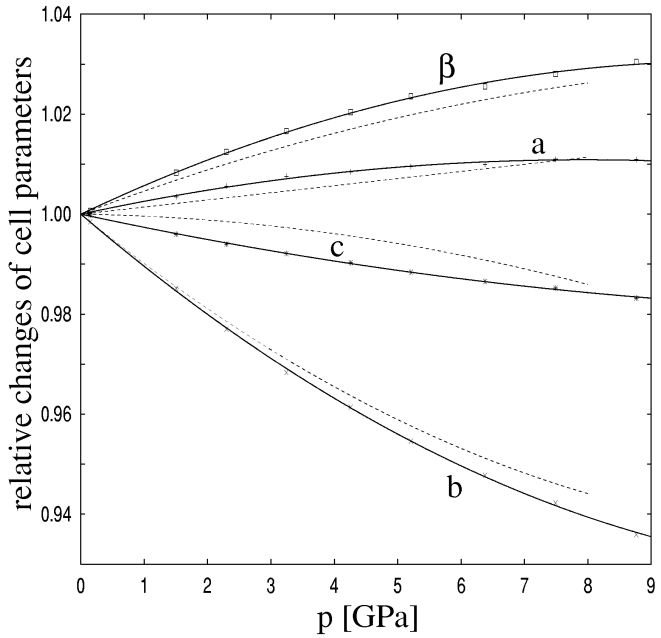

Figure 3. Relative changes of the lattice parameters as a function of pressure. The full lines are fits to the data in this work; the dashed lines refer to the fits to reported single-crystal synchrotron data [7].

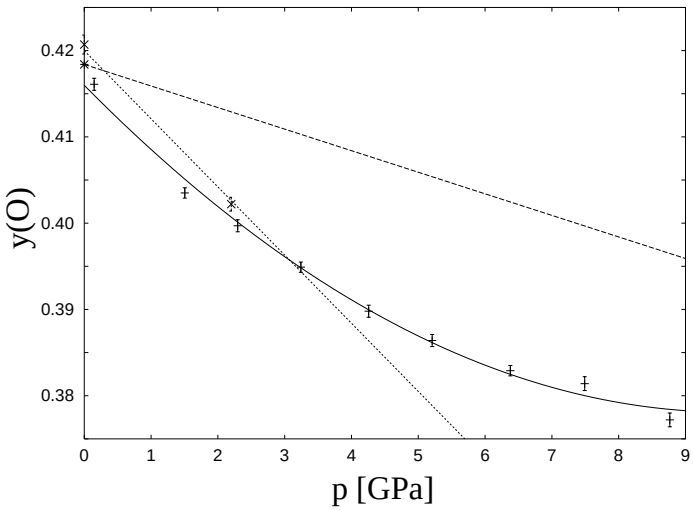

Figure 4. Pressure dependence of the oxygen positional parameter y(O). The smooth curve is the fit according to equation (1) with the coefficients in table 3, and the dotted line indicates the linear fit obtained from one previous high-pressure neutron experiment [9]. The dashed line represents the proposed linear dependence used to explain the pressure-induced shifts in Raman modes [8].

$\partial y(\mathrm{O})/\partial p = -0.0079(6)$ GPa^{-1} obtained from the previous neutron study [9] offers only an approximate description to pressures up to 4 GPa. Clearly, the analysis of the Raman

experiments [8] has to be reconsidered in the light of these new results, which offer complete structural information up to 9 GPa.

The experimental values $V(p)$ in table 1 can be fitted by a Birch equation of state:

$$p = \frac{K_0}{K_0'}\left[\left(\frac{V_0}{V}\right)^{K_0'} - 1\right] \tag{2}$$

and are in agreement within uncertainties for $K_0 = 72(2)$ GPa, $K_0' = 8.7(1.2)$ and $V_0 = 80.89(5)$ Å^3; see figure 5.

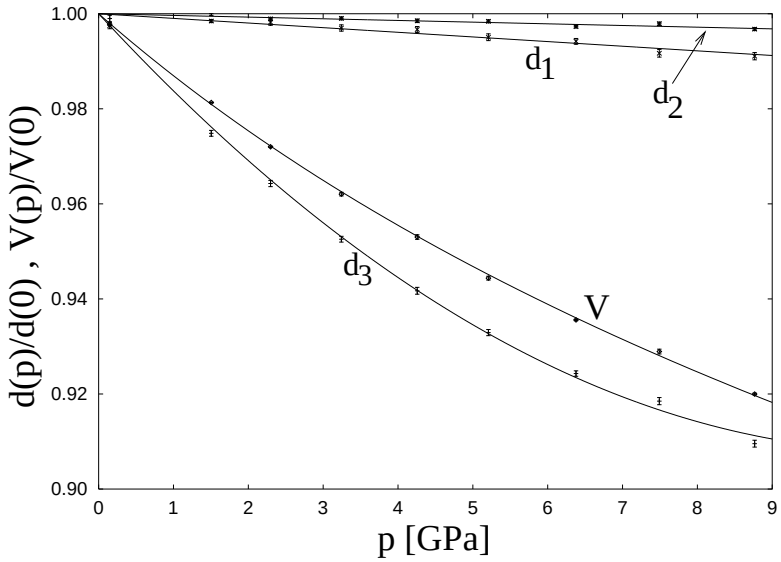

Figure 5. Relative compression of the three non-equivalent Cu–O bonds in CuO. The fits are according to equation (1) with the coefficients given in table 3. In addition, the Birch equation of state (equation (2)) is shown together with the experimental cell volume data.

The compressibilities of the two short Cu–O bonds are constant in the pressure range up to 9 GPa, while pronounced deviations from a linear behaviour $d(p)$ are observed for the third bond, which is elongated due to the Jahn–Teller effect; see figure 5. Using a two-term bond potential model, the pressure dependence of compressibility is fitted by

$$\kappa(p) = 0.0710(55)/(p + 3.15(55)\ \text{GPa}). \tag{3}$$

See equations (6-9) and (7-9) in [14]. The effect of applied pressure on the crystal structure of CuO is to make the octahedra more regular as shown for three representative angles; see figure 6. However, the crystal structure cannot be transformed into the regular rock-salt structure by a continuous displacive second-order phase transition: this would require a first-order transition.

The compressibilities of copper(II)–oxygen bonds are in general strongly dependent on the specific structural environment. Nevertheless, to a first approximation, it is useful to compare bond compressibilities in similar compounds with respect to the specific bond length. Figure 7 summarizes the observed compressibilities κ of several copper oxides as a function of bond length. Error bars are only given for the elongated bonds in coordination polyhedra with coordination number CN $= 5$ or 6, because the compressibilities of the four short bonds are generally very imprecise as the changes in bond length are comparable to the experimental uncertainties. The compounds $HgBa_2Ca_{n-1}Cu_nO_{2n+2+\delta}$ with $\langle d\rangle = 2.7744$ Å

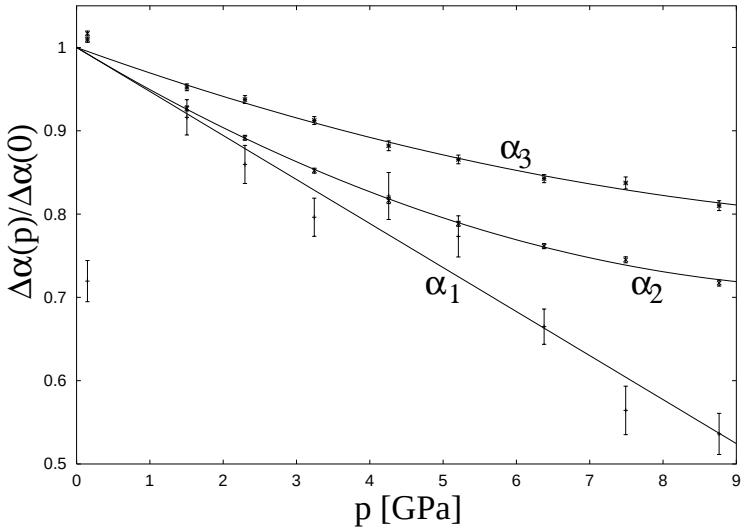

Figure 6. Reduction of the deviation from 90° by the application of pressure for three representative bond angles in CuO. For the definition of α_1, α_2 and α_3, see figure 1.

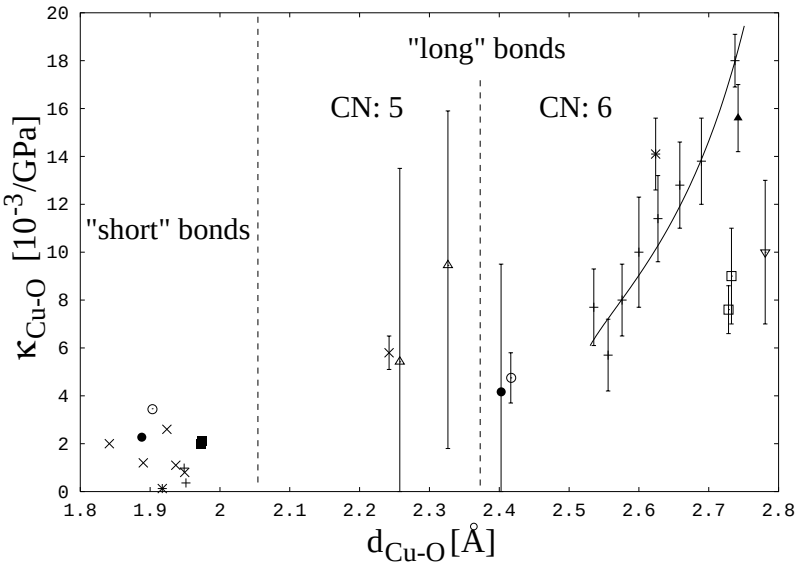

Figure 7. Compressibility of Cu(II)–O bonds versus corresponding bond length for different compounds: CuO (+) this work, CuO (closed triangle) [9], $YBa_2Cu_3O_{7-x}$ (open triangles) [1], $CuGeO_3$ (asterisk) [16], $Nd_{2-x}Ce_xCuO_4$, $x = 0$ and 0.165, respectively (closed squares) [17], $HgBa_2CuO_{4+\delta}$, $\delta \sim 0.12$ (open squares) [18], (open triangle, tip down) [15], $YBa_2Cu_4O_8$ (times sign) [19], $La_{2-x}Sr_xCuO_4$, $x = 0$ (open circles) [20] and $x = 0.15$, respectively (closed circles) [21].

and $\kappa = 14.0(4.4) \times 10^{-3}$ GPa^{-1} for $n = 1$ and $\langle d \rangle = 2.758$ Å and $\kappa \sim 0$ for $n = 2$ [15] with CN = 5 have an anomalously long Cu–O bond due to the strong Hg–O bond present and are not included in figure 7. By combining $\kappa(p)$ (equation (3)) and $d(p)$ (equation (1) and

table 3) the $\kappa(d)$ dependence can be plotted for CuO and provides an approximate estimate for bond compressibilities of the Jahn–Teller elongated bonds in [CuO_6] octahedra in other compounds.

Acknowledgments

Financial support from the European Commission by a Marie Curie fellowship for HE is gratefully acknowledged. We thank Duncan Francis for technical support and the EPSRC for provision of beam time at ISIS and a studentship for JAM.

References

[1] Jorgensen J D, Pei S, Lightfoot P, Hinks D G, Veal B W, Dabrowski B, Paulikas A P, Kleb R and Brown I D 1990 *Physica* C **171** 93–102
[2] Zhu Y T and Manthiram A 1994 *Phys. Rev.* B **49** 6293–8
[3] Zhou J-S, Chen H and Goodenough J B 1994 *Phys. Rev.* B **49** 9084–90
[4] van Loodsrecht P H M, Zeman J, Martinez G, Dhalenne G and Revcolevschi A 1997 *Phys. Rev. Lett.* **78** 487–90
[5] Tunell G, Posnjak E and Ksanda C J 1935 *Z. Kristallogr.* **90** 120–42
[6] Åsbrink S and Norrby L-J 1970 *Acta Crystallogr.* B **26** 8–15
[7] Malinkowski M, Åsbrink S and Kvick Å 1990 *High Pressure Res.* **4** 429–31
[8] Reimann K and Syassen K 1990 *Solid State Commun.* **76** 137–40
[9] Forsyth J B and Hull S 1991 *J. Phys.: Condens. Matter* **3** 5257–61
[10] Besson J M, Nelmes R J, Hamel G, Loveday J S, Weill G and Hull S 1992 *Physica* B **180+181** 907–10
[11] Wilson R M, Loveday J S, Nelmes R J, Klotz S and Marshall W G 1995 *Nucl. Instrum. Methods* A **354** 145–8
[12] Larson A C and von Dreele R B *General Structure Analysis System* LANSCE, Los Alamos National Laboratory, NM
[13] Decker D L 1971 *J. Appl. Phys.* **42** 3239–44
[14] Hazen R M and Finger L W 1982 *Comparative Crystal Chemistry* (Chichester: Wiley)
[15] Hunter B A, Jorgensen J D, Wagner J L, Radaelli P G, Hinks D G, Shaked H, Hitterman R L and Von Dreele R B 1994 *Physica* C **221** 1–10
[16] Bräuninger S, Schwarz U, Hanfland M, Zhou T, Kremer R K and Syassen K 1997 *Phys. Rev.* B **56** R11 357–60
[17] Kamiyama T, Izumi F, Takahashi H, Jorgensen J D, Dabrowski B, Hitterman R L, Hinks D G, Shaked H, Mason T O and Seabaugh M 1994 *Physica* C **229** 377–88
[18] Aksenov V L, Balagurov A M, Savenko B N, Sheptyakov D V, Glazkov V P, Somenkov V A, Shilshtein S Sh, Antipov E V and Putilin S N 1997 *Physica* C **275** 87–92
[19] Nelmes R J, Loveday J S, Kaldis E and Karpinski J 1990 *Physica* C **172** 311–24
[20] Takahashi H, Shaked H, Hunter B A, Radaelli P G, Hitterman R L, Hinks D G and Jorgensen J D 1994 *Phys. Rev.* B **50** 3221–9
[21] Pei S, Jorgensen J D, Hinks D G, Dabrowski B, Lightfoot P and Richards D R 1990 *Physica* C **169** 179–83